Quantum mechanics of highly excited states of the H+ 3 molecular ion: A numerical study of the two degree of freedom C 2v subspace

Jonathan Tennyson, Otto Brass, and Eli Pollak

Citation: The Journal of Chemical Physics **92**, 3005 (1990); doi: 10.1063/1.457896
View online: http://dx.doi.org/10.1063/1.457896
View Table of Contents: http://scitation.aip.org/content/aip/journal/jcp/92/5?ver=pdfcov
Published by the AIP Publishing

Quantum mechanics of highly excited states of the H_3^+ molecular ion: A numerical study of the two degree of freedom C_{2v} subspace

Jonathan Tennyson,[a] Otto Brass, and Eli Pollak
Chemical Physics Department, Weizmann Institute of Science, Rehovot 76100, Israel

(Received 27 June 1989; accepted 27 October 1989)

Two degrees of freedom quantum mechanical calculations on the bound states of H_3^+ are presented. Two different potential energy surfaces are employed. The effect of rotational excitation is analyzed. For $J = 0$, the high energy region is composed largely of states that cannot be assigned. However, two regularly spaced series are observed, corresponding to "horseshoe" states predicted previously by classical calculations. In addition we find a new assignable series of inverted hyperspherical states. Conversely, for high orbiting angular momentum ($l = 20$) in which the proton rotates about the diatom, assignable normal mode states persist up to dissociation. Semiclassical periodic orbit quantization is found to give excellent agreement for the regular quantum states. The significance of these results for the interpretation of the H_3^+ photodissociation spectrum is discussed.

I. INTRODUCTION

The H_3^+ molecule ion has been studied extensively by experimentalists[1] and theorists[2] in the past decade. Oka and co-workers have measured precisely the fundamental and low overtone vibration–rotation spectrum. Meyer and co-workers[3] have computed several potential energy surfaces and corresponding (numerically converged) fundamentals. Using their best surface (the MBB potential), Miller and Tennyson[4] and Whitnell and Light[5] have computed the overtone spectrum. The spectroscopy of H_3^+, up to an energy of approximately 1.2 eV above the ground state, is reasonably well understood.

The situation is quite different for energies which are close to the dissociation threshold energy into $H_2 + H^+$. Five years ago, Carrington and Kennedy[6] published the results of a detailed measurement of the photodissociation spectrum of H_3^+. Their experiment, which was limited to a very narrow spectral range of 220 cm^{-1}, revealed over 27 000 sharp transitions of the ion at energies which are within 1000 cm^{-1} of the dissociation energy. A spectroscopic assignment of all these lines seems at present to be hopeless. However, when Carrington and Kennedy coarse grained their spectrum they found an amazing regular pattern. The detailed spectrum collapsed into four equally spaced lines.

The high energy and high density of states suggest at first glance that a full three-dimensional quantum mechanical analysis is at present not yet feasible. A model quantum mechanical study by Pfeiffer and Child[7] gave the correct density of lines but did not explain the regular coarse grained spectrum. Schlier and co-workers[8] embarked on a classical mechanical study of the system. Their study also accounted for the correct density of states, moreover, at zero total angular momentum, they discovered a stable periodic orbit, which was nicknamed the "horseshoe" orbit. This orbit, has a C_{2v} symmetry, the motion along this orbit can be thought of as a highly excited bending motion of the central atom in a quasilinear molecule. Gomez and Pollak[9] showed that this orbit retains its C_{2v} symmetry and stability, when the outer two atoms are rotated in a plane perpendicular to the symmetry line. The rotational constant of the rotating horseshoe orbit was found to be 30 cm^{-1}. This led Gomez and Pollak to assign the coarse grained experimental spectrum as the R branch spectrum of the antisymmetric stretch (ν_3) mode of the rotating horseshoe orbit.

These classical mechanical studies raise some questions. Except for the rotating horseshoe orbit, to date, no other stable orbit has been found in the experimental energy and total angular momentum range. This means that predominantly, the classical dynamics are chaotic. In fact, the regular phase space around the horseshoe orbit is very small and not enough for EBK quantization. The relationship between a single orbit and the exact quantum mechanics of such a strongly coupled system is not yet clear. Taylor and co-workers,[10] have suggested that the stable periodic orbit identifies a relatively decoupled region of phase space which can cause a quantum mechanical resonance. Using a Feshbach formalism and local basis functions, they identify this localized resonance state as a P state which interacts with the background quasicontinuum states leading to a Lorentzian peak in a coarse grained spectrum. Using a stabilization method they have studied the two degree of freedom C_{2v} Hamiltonian and found states that localize around the rotating horseshoe orbit. [10(b)] Moreover, they found agreement between semiclassically quantized energies of the rotating horseshoe and the energies of the stabilized eigenvalues.

Manz and co-workers have in recent years studied in detail the quantum mechanical scattering resonances for a collinear ABA molecule moving on a coupled Morse potential.[11] They found that the resonant wave functions, can be identified as hyperspherical modes. Stefanski and Pollak[12] have shown that the wave functions localize around a hyperspherical like stable periodic orbit. An EBK quantization of the orbit which is based on the action of the orbit and its stability frequency gave excellent agreement with quantum

[a] Permanent address: Dept. of Physics and Astronomy, University College London, London WC1E 6BT, England.

 0021-9606/90/053005-13$03.00

resonance energies. Here too, the stable phase space surrounding the orbit was smaller than $\hbar$.

It is not an accident that the converged 3D quantum studies of the H_3^+ molecular ion have not gone substantially beyond 1.2 eV. This energy is approximately the saddle point energy of collinear H_3^+. Above this energy, the molecule becomes quite floppy, the density of states increases rapidly and the basis set becomes unmanageable. All the previous studies imply that even only qualitative insight into the high energy spectrum of H_3^+ demands an exact quantal analysis of states which are above the collinear threshold. As a first step in this direction we report in this paper a detailed converged numerical study of all bound states of H_3^+ restricted to the two degree of freedom C_{2v} geometry. We will show that already slightly above the collinear saddle point one finds quantum states that localize around the horseshoe orbit. The horseshoe orbit is a source for a ladder of states which can be assigned. The resonance horseshoe states found by Taylor and co-workers[10(b)] are the extension of the horseshoe states to energies above dissociation. We also find an additional ladder of states which localize around a different orbit, which may be characterized as an inverted hyperspherical mode. This orbit is though not as stable as the horseshoe orbit.

In Sec. II we describe the details of the quantum computations and provide figures of the various types of quantum states found. A semiclassical analysis of the quantum states, based on stability analysis of the stable orbits is provided in Sec. III. The semiclassical analysis[13] provides a simple and useful assignment of many states but not all of them. Implications of this work on the full 3D dynamics as well as on the analysis of the coarse grained photodissociation spectrum are discussed in Sec. IV.

II. QUANTUM MECHANICAL CALCULATIONS

A. Methodology

The classical mechanical Hamiltonian for the motion of H_3^+ restricted to C_{2v} symmetry takes two forms. Using Jacobi coordinates, where r is the internuclear separation of the H_2 diatom and R is the distance of the third atom from the H_2 center, one distinguishes between a rotational (H_j) and an orbiting (H_l) Hamiltonian.[9(b)] The rotational Hamiltonian is written as

$$H_j = \frac{1}{2\mu_1} p_r^2 + \frac{1}{2\mu_2} p_R^2 + \frac{j^2}{2\mu_1 r^2} + V(r,R,\theta = \pi/2), \tag{1}$$

where (p_r,p_R) are the momenta conjugate to the coordinates (r,R), the angle θ between r and R is fixed at 90°, μ_1 is the H_2 reduced mass $(m_H/2)$ and μ_2 is the reduced mass of the complex $(2m_H/3)$. This Hamiltonian corresponds to rotating the H_2 diatom such that its angular momentum j is along the R axis and coincides with the total angular momentum J. Here the atom to diatom distance R may be thought of as a Cartesian coordinate with the range $(-\infty,\infty)$. One may also rotate the proton about the H_2 diatom such that the angular momentum l is along the r axis. In this case one obtains the orbiting Hamiltonian:

$$H_l = \frac{1}{2\mu_1} p_r^2 + \frac{1}{2\mu_2} p_R^2 + \frac{l^2}{2\mu_2 R^2} + V(r,R,\theta = \pi/2). \tag{2}$$

The quantum mechanical Hamiltonian is obtained by replacing the classical momentum operator with the quantum analog $[-i\hbar(\partial/\partial x), x = r,R]$ and the angular momenta j^2, l^2 by $\hbar^2 j(j+1)$, $\hbar^2 l(l+1)$, respectively.

Our main interest lies in the bound states whose energies lie between the collinear threshold and the $H^+ + H_2$ dissociation threshold. In this region, the molecule is rather extended and floppy so that the standard basis sets used previously must be somewhat modified. Solutions for the 2D problem were found using a basis set expansion of the form

$$\Psi(r,R) = \sum_{m,n} \chi_m(r)\chi'_n(R). \tag{3}$$

For the r motion, the Tennyson–Sutcliffe[14] Morse oscillator-like functions were used. These functions are however inappropriate for the R coordinate. The reduced Hamiltonian is symmetric with respect to reflection about $R = 0$. This means that eigenstates separate into even and odd states with respect to reflection. The Morse eigenfunctions are poorly adapted for this property, they have the wrong boundary condition at $R = 0$. Instead we use spherical oscillator functions (cf. Ref. 15).

The Morse and spherical oscillator functions have parameters which arise from the specific form of the 1D Hamiltonian that defines them. In this work, these parameters were treated as variational parameters to give an optimized basis set for the system. The parameters were varied for each coordinate on a trial and error basis until satisfactory convergence was obtained for a moderate basis. These tests showed that parameters used previously[4] for the r coordinate were satisfactory only for very low-lying states. The optimal parameters (in atomic units) were found to be $r_e = 2.86$, $\omega_e = 0.0075$, and $D_e = 0.11$ for the Morse-like functions, and $\alpha = 0.0$, $\omega_e = 0.0225$ for the spherical oscillators. These parameters differ markedly from previous optimizations used for converged low energy 3D computations.

Because of the symmetry of the Hamiltonian it suffices to diagonalize it in the range $R = 0,\infty$, with either odd or even oscillator functions.

In this paper we restrict ourselves to the odd functions. There are not any major qualitative differences between them and the even functions. Test calculations with $l = j = 0$ showed that a basis of 31 spherical oscillators and 23 Morse-like functions was sufficient to converge the lowest 120 states to within 2 cm^{-1} and remaining states below the dissociation energy to about 5 cm^{-1}. No attempt was made to look for diffuse states lying just below dissociation.

Two potential energy surfaces were used. The DIM potential[16] has the advantage that it is well defined, with continuous first derivatives for all energies leading to the three-body dissociation limit. It is not an *ab initio* surface and so not spectroscopically accurate. However the dissociation energies, fundamental frequencies, and collinear saddle point energy are in fair agreement with *ab initio* computations so that one expects this surface to reveal the important qualitative features of excited H_3^+. The other surface, denoted

MBB,[3] is a highly accurate *ab initio* potential energy surface and has been used[4] to predict experimental spectroscopic lines with an accuracy of 0.2 cm^{-1}. Unfortunately, a good interpolation function for the *ab initio* points exists only up to 25 000 cm^{-1}. Below this energy the two surfaces are quite similar so that the basis set chosen is equally well adapted for both potentials.

B. Results

With the basis set described above, it was possible to obtain almost all converged energies and wave functions, below the $H^+ + H_2$ dissociation threshold, for all j,l values of rotating and orbiting H_3^+ in the C_{2v} configuration. This leads to an enormous amount of data and the necessity of compaction. The general structure of the wave functions, from the ground state to the dissociation threshold, does not change drastically with different values of the rotational angular momentum quantum number j. Therefore we chose to present in great detail only the results for nonrotating H_3^+. In Fig. 1 we plot 128 bound states. The coordinates are mass scaled to allow easy comparison with periodic orbits. The outer dashed line in each panel denotes the boundary of the classically allowed region of configuration space at the energy of the state. All states shown are odd with respect to reflection about $R = 0$.

The symmetric stretch mode is along the line $\tilde{r} = \tilde{R}$. The motion perpendicular to the symmetric stretch is a bending mode. The antisymmetric stretch motion is not allowed for the restricted symmetry C_{2v} geometry. Inspection of the 13 lowest lying states shows that they are easily assigned in terms of the normal modes, (ν_1,ν_2) which correspond to the symmetric and bending modes, respectively. It is interesting to note that the fundamental frequencies obtained from the 2D computation are very close to the fully coupled[3] (3D) results. This indicates that at low energies the antisymmetric stretch (ν_3) is nearly decoupled from the other modes.

As soon as one reaches the collinear ($R = 0$) threshold, assignment becomes no longer trivial. Note, that the collinear threshold is easily discerned from the equipotential contour of the state which becomes open for energies above the threshold. From this point onwards, the wave functions become interesting. It becomes impossible to assign many states. As energy increases, the density of unassignable states increases quite rapidly. However, one still finds at regular energy intervals some states which are highly localized. One set can be called "horseshoe" states, if one plots their reflection for negative R, one obtains a horseshoe-like shape. These states are an extension of the bending mode from energies below the collinear threshold to energies above the threshold and so can be assigned as highly excited ν_2. It is also evident that these horseshoe states exist with low excitations along the symmetric stretch (ν_1) mode. Clear examples are states 50 and 60 where one discerns a single nodal line along the bending direction. As energy increases, more excitations stabilize, state 114 has two excitations along the ν_1 mode, state 103 seems to have 3.

The second type of localized states may be thought of as inverted hyperspherical modes, using the terminology of Manz and co-workers.[11] Some clear examples are states 109 and 124. One notes that they are to a large extent localized around an almost circular arc, so they can be called hyperspherical. However the origin of the circle is not at the origin of the coordinate system, the arc is convex with respect to the origin, hence the adjective inverted. The hyperspherical modes appear only at quite high energies, they do not appear to be stable enough to support excitations perpendicular to the hyperspherical mode.

All states plotted in Fig. 1 are for the DIM potential energy surface. Numerical details such as energies and assignments are provided in Table I. For the interpretation of the coarse grained photodissociation spectrum it is of interest to know the rotational constants associated with each state. The two rotational constants appearing in the Table are defined as

$$B_j = \left\langle \frac{\hbar^2}{2\mu_1 r^2} \right\rangle, \quad B_l = \left\langle \frac{\hbar^2}{2\mu_2 R^2} \right\rangle, \tag{4}$$

where the brackets denote an average over the wave function. Large variations are found for the orbiting constant B_l, generally, horseshoe states have large values of B_l owing to their nonnegligible density around $R = 0$. Here we note that for even functions, B_l diverges at $l = 0$. Perhaps the most interesting result is the fact that the rotational constant B_j fluctuates only slightly about an average value of $\sim 30\ cm^{-1}$ for all states. It is also of interest to note that the rotational constant of inverted hyperspherical states is generally somewhat larger than the B_j of horseshoe states.

Analogous results for the MBB potential energy surface are presented in tabular form in Table II. There are no strong qualitative differences between the results for both potentials. The assignments given for the MBB states are obtained from inspection of the wave functions, just as for the DIM surface. Because of the qualitative similarity we do not show the plots. The density of states on both surfaces is quite similar, the ν_1 fundamental is somewhat lower on the MBB surface but the ν_2 fundamental is somewhat higher and there seems to be a compensation. The main notable difference is that the MBB surface seems to be more regular in the sense that more states can be assigned, one finds a larger number of states with ν_1 excitations of the horseshoe mode. However, the inverted hyperspherical mode does not allow for perpendicular excitations and we do not find any additional different qualitative type of localized state.

As mentioned, rotational (j) excitation does not affect the qualitative structure of the wave functions. In Table III we summarize the energies and rotational constants for some j-rotating states that belong to the horseshoe family. One notes that the vibrational spacing does not change much with j. As in the $j = 0$ case, one finds many horseshoe states with excitations in the ν_1 direction. As j increases, these excitations seem to be stabilized so that more states can be assigned. Interestingly, the rotational constant B_j is a decreasing function of j. This is a result of the centrifugal force which tends to separate the H_2 diatom to larger distances.

Excitation of orbital (l) angular momentum changes the whole picture dramatically. Any infinitesimal amount of orbital angular momentum causes a divergence of the effective potential energy surface at $R = 0$ preventing the motion

through the center of the diatom. This added repulsive wall seems to stiffen the molecule considerably. One finds a noticeable decrease in the density of states. Perhaps the most important difference is that almost all bound states can be assigned by the time the orbital angular momentum reaches a value of 20. In Fig. 2, we plot all the bound states of orbiting H_3^+ at $l = 20$. One immediately notes that the normal mode assignments stay valid up to very high energy. There is no need to talk here of a horseshoe mode, the repulsive wall at $R = 0$ makes the horseshoe identical to high excitation in the ν_2 mode.

Numerical data, normal mode assignments and rotational constants for all bound $l = 20$ states are provided in Table IV. The rotational constants for the orbiting states do not change much with energy. However, the orbiting constant (B_l) depends strongly on l. For $l = 0$, one notes from Table I that B_l is large and fluctuates with energy. When motion is allowed through $R = 0$, one expects a large constant. Since the orbiting motion prevents the system from coming close to the collinear configuration, the constant becomes substantially smaller and rather insensitive to energy. Clearly, by varying l one can obtain quite a large range of possible B_l values. The rotational constant B_j increases somewhat with l, the orbiting motion pulls the atom away from the diatom enabling the distance of the diatom to become shorter, thus increasing the constant.

III. SEMICLASSICAL ANALYSIS

Periodic orbits can be found for the two degree of freedom Hamiltonian using the turning point method detailed in Ref. 17. The search procedure allows for a highly accurate determination of the initial point of the orbit. The period of the orbit is evaluated using a variant of the Hénon method,[18] for an accurate stability analysis it is important to have a highly accurate estimate of the period. Given these it is straightforward to find the Liapunov exponents and stability frequencies of the orbits. Technical details on stability analysis may be found for example in Ref. 17.

For a stable orbit, one may use the action of the orbit and its stability frequency to predict quantum mechanical bound state energies. The motion along the orbit is quantized using the WKB estimate:

$$\oint \mathbf{p}\cdot d\mathbf{q} = (n + 1/2)2\pi\hbar, \tag{5}$$

where the integral is along the periodic orbit. This condition defines a quantized energy E_n^{PO}. To this energy one must add the quantized energy of the perpendicular mode, which is obtained using a harmonic approximation based on the stability frequency of the orbit (ω_s^n) at the energy E_n^{PO}. Thus the energy of the (m,n) state associated with a given family of orbits is given by the semiclassical formula:

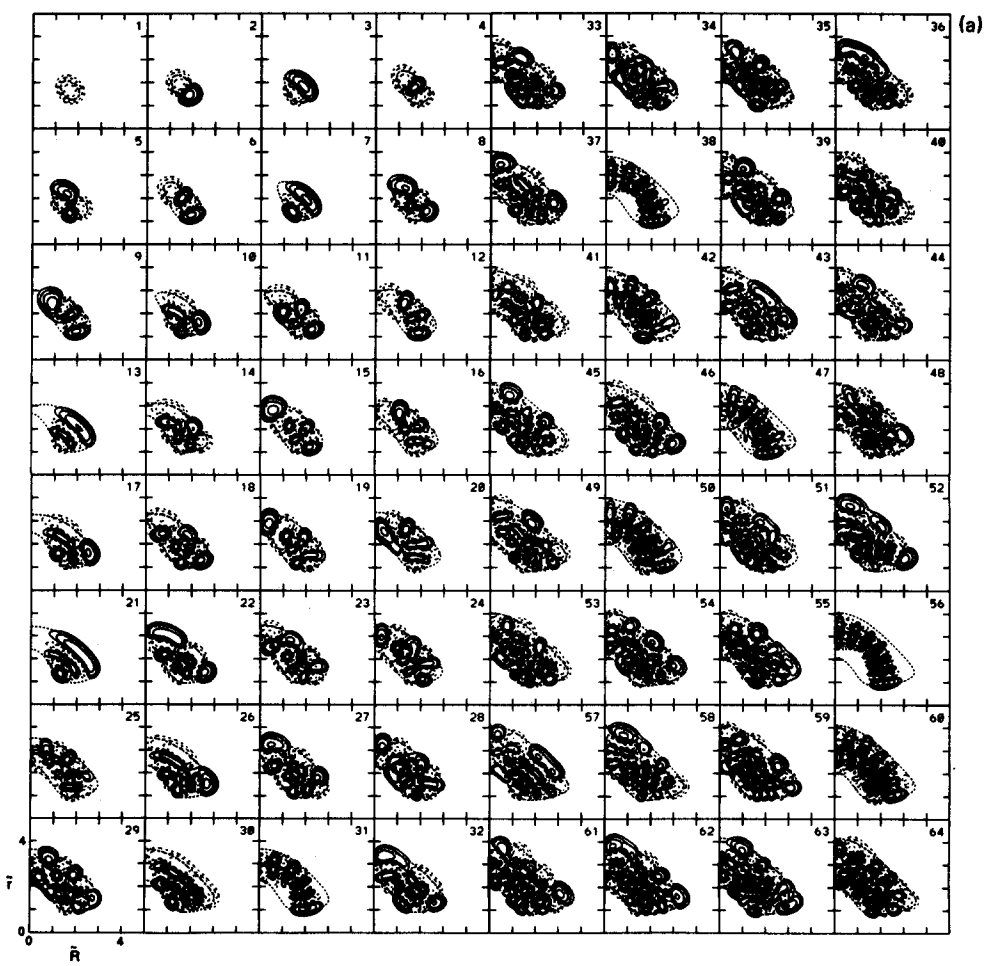

FIG. 1. Odd bound states of (C_{2v}) H_3^+ ($j = l = 0$) on the DIM potential energy surface. The mass weighted coordinates $\tilde{r},\tilde{R}$ are defined as $\tilde{r} = \alpha r$, $\tilde{R} = R/\alpha$, $\alpha = (\frac{3}{4})^{1/4}$. The dashed boundary line denotes the classically allowed region of configuration space at the energy of the eigenvalue. Dashed and solid contours show negative and positive values of the wave function, respectively. Contours are for 0.64, 0.32, 0.16, and 0.08 of the maximum amplitude. The heavy solid lines shown for states 25, 31, 38 ··· are the horseshoe orbits that quantize these states.

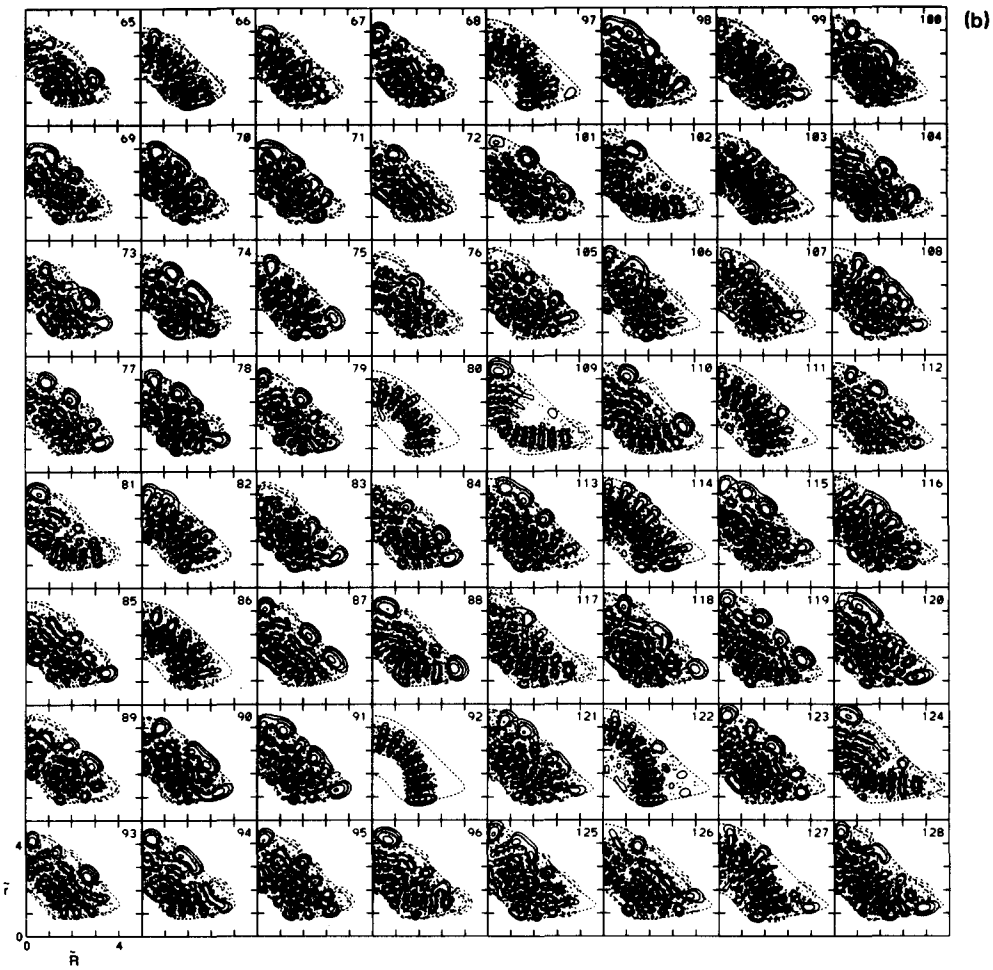

FIG. 1 (continued).

$$E_{m,n} = E_n^{\mathrm{PO}} + \hbar\omega_s^n(m + 1/2). \tag{6}$$

This very simple method of estimation has been tested on a number of systems[12,13] and shown to be quite accurate for states whose excitation in the direction perpendicular to the orbit is low. Here it is important to stress that this method is useful even when this excitation far exceeds the regular region of phase space surrounding the orbit. As has been noted in a recent paper,[12] quantum localization is much stronger than classical localization.

There is though one technical problem in practical application of the method. Within the Liapunov stability analysis the phase is determined only up to multiples of 2π. In order to know the absolute phase, one has two choices. A method used previously[13] is to compute the eigenvalues continuously from a known limit, for example from the bottom of a potential energy well where a harmonic analysis provides the absolute phase. This procedure is inapplicable in our case, where the horseshoe orbit does not exist at energies lower than the collinear threshold. The alternative method used in this paper is to follow the number of crossings of a trajectory adjacent to the periodic orbit. For the horseshoe orbit there are five crossings within one period indicating that the stability frequency is given as

$$\omega_s^n = \frac{1}{T_n}\left[5\pi + tg^{-1}(\mathrm{Im}\,\lambda_n/\mathrm{Re}\,\lambda_n)\right], \tag{7}$$

where λ_n is the characteristic eigenvalue and T_n the period of the quantized orbit.

In Table V we provide the energy dependence of the action, period and (absolute) stability frequencies of the horseshoe orbits for a number of j values. In addition, we determined the rotational constants B_j [cf. Eq. (4)] which are obtained by averaging over one period of the orbit. All these quantities vary smoothly with energy so that a linear interpolation between the energies in the Table is very accurate. In the previous section we provided the quantized energies predicted from the horseshoe orbits and compared with the exact quantal results. The agreement is amazingly accurate especially when there is no excitation in the perpendicular (ν_1) mode. In Fig. 1 we also plotted the quantized orbits for each of the quantum horseshoe states. One notes the localization of the quantum wave functions around the quantized orbits.

In Fig. 3(a) we plot the exact quantum energy vs the semiclassical prediction for all assignable quantum horseshoe states at $j = l = 0$. Ideally, this should give a straight line with unit slope. In Fig. 3(b) we plot the absolute energy

TABLE I. Converged quantum mechanical eigenvalues for nonrotating (C_{2v}) H_3^+ on the DIM potential energy surface. All energies are in cm^{-1}, relative to the quantum mechanical ground state whose zero point energy is 2924.83 cm^{-1}. E_Q are the quantum energies, E_{SC} are the semiclassical predictions based on horseshoe quantization (cf. Sec. III). The rotational constants B_j, B_l are defined in Eq. (4) and given in units of cm^{-1}. The assignment (ν_1, ν_2) refers to the symmetric and bend normal modes respectively and is based on node counting in the contour plots. Question marks imply imperfect nodal lines, but are *not* meant to cast doubt on the assignment. Assignments marked (ν_1,ν_2)* refer to the inverted hyperspherical mode where ν_2 is the quantum number perpendicular to the mode.

N	E_Q	E_{SC}	B_j	B_l	(ν_1,ν_2)	N	E_Q	E_{SC}	B_j	B_l	(ν_1,ν_2)
1	0.0		38.54	41.19	0, 0	48	19949.4		28.29	458.82	
2	2229.9		36.91	45.93	0, 1	49	20268.2		29.47	272.38	
3	3382.3		37.89	40.68	1, 0	50	20565.2	20648.0	30.49	884.78	1,10
4	4335.1		35.10	53.16	0, 2	51	20684.7		29.78	452.13	
5	5481.7		36.24	46.01	1, 1 ?	52	20886.0		29.02	357.42	14, 0* ?
6	6298.5		33.08	65.73	0, 3	53	21292.1		28.91	365.70	
7	6674.8		37.20	40.33	2, 0	54	21454.6		30.81	401.15	
8	7464.0		34.36	55.61	1, 2 ?	55	21526.2		28.50	634.02	
9	8097.6		30.81	94.38	0, 4	56	21795.8	21807.9	31.90	1007.81	0,12
10	8630.8		35.48	47.10	2, 1 ?	57	21930.8		31.71	193.10	
11	9297.2		31.88	89.20	1, 3 ?	58	22066.0		27.60	405.05	15, 0* ?
12	9717.6		28.73	178.72	0, 5	59	22362.6		30.61	383.14	
13	9873.2		36.44	40.49	3, 0	60	22466.2	22562.0	31.13	936.76	1,11
14	10473.9		33.32	66.35	2, 2 ?	61	22571.2		29.36	475.89	
15	10920.5		28.95	277.41	0, 6 ?	62	22889.0		27.93	336.18	
16	11249.8		28.52	267.64	0, 6	63	23172.9		29.25	636.36	
17	11664.5		34.44	52.30	3, 1 ?	64	23271.4		28.51	689.44	
18	12144.1		30.23	178.85	2, 3 ?	65	23332.5		30.99	313.21	
19	12476.5		29.29	460.66	0, 7 ?	66	23838.3	23861.4	31.13	819.46	0,13 ?
20	12775.0		27.98	350.68	0, 7	67	23857.0		30.31	620.22	
21	12964.3		35.40	43.39	4, 0	68	23996.9		30.30	416.94	
22	13347.3		31.71	116.48		69	24148.0		28.19	622.79	
23	13674.5		29.37	358.70		70	24421.7		29.20	659.44	
24	14115.9		29.45	444.15		71	24444.6		29.88	681.98	
25	14305.2	14250.9	28.29	573.69	0, 8	72	24601.5		30.15	267.12	
26	14549.7		32.61	84.48	9, 0 ?	73	24956.4		30.29	418.29	
27	14879.0		29.71	267.76		74	25013.3		31.09	502.44	
28	15267.7		29.95	436.84		75	25082.4		30.42	816.97	
29	15670.1		28.05	359.10		76	25348.7		26.86	477.19	
30	15888.9		32.67	85.58	5,0 ?	77	25647.6		28.84	348.00	
				or	10,0* ?	78	25798.7		30.42	576.68	
31	15992.0	15987.6	29.87	855.30	0, 9	79	25846.8		29.23	602.15	
32	16114.6		31.23	208.81		80	25924.1	25937.8	32.11	1027.96	0,14
33	16416.9		30.69	322.33		81	26212.8		30.02	435.99	19, 0*
34	16902.2		29.46	496.38		82	26431.9		30.75	875.23	
35	17168.9		28.47	487.62		83	26499.1		28.70	666.25	
36	17242.4		29.89	193.83	11, 0* ?	84	26586.5		30.20	404.26	
37	17589.1		30.21	267.05		85	26869.3		27.22	448.57	
38	17844.6	17851.5	30.87	931.47	0,10	86	26980.1	27263.6	31.24	946.18	2,12
39	18008.7		30.16	425.20		87	27124.3		29.02	393.43	
40	18388.7		28.57	375.38		88	27330.6		30.75	445.25	20, 0* ?
41	18610.7		29.50	232.37		89	27497.7		28.57	561.33	
42	18777.0	18823.2	29.33	759.29	1, 9 ?	90	27565.1		30.58	517.17	
43	18861.2		31.26	297.34		91	27674.9		28.78	588.08	
44	19174.1		31.77	227.92		92	28002.2	28019.5	32.15	1038.53	0,15
45	19582.1		28.74	490.78		93	28164.4		29.29	341.12	
46	19780.8		30.09	324.63		94	28224.6		30.26	434.98	
47	19790.1	19803.0	31.40	946.43	0,11	95	28297.9		29.4	689.33	

TABLE I (*continued*).

N	E_Q		E_{SC}	B_j	B_l (ν_1,ν_2)	N	E_Q		E_{SC}	B_j	B_l (ν_1,ν_2)
96	28417.4		29.39	537.31	21, 0* ?	123	32161.3		29.86	484.62	
97	28516.6	28631.1	31.98	1010.71	1,14	124	32304.4		31.92	434.73	25, 0* ?
98	28776.4		26.64	469.13		125	32421.4		27.88	727.16	
99	28948.4	29273.9	31.41	845.75	2,13 ?	126	32496.9		30.53	389.31	
100	29028.2		30.45	504.11		127	32658.7	32772.4	31.80	938.27	1,16 ?
101	29302.9		28.64	513.17		128	32671.9		29.83	627.80	
102	29383.6		30.79	527.76	22, 0* ?	129	32921.7		28.55	516.64	
103	29441.7	29991.4	30.40	871.97	3,12 ?	130	33023.2		31.15	661.24	
104	29565.4		26.62	459.45		131	33050.3		31.71	748.19	
105	29817.6		29.14	492.93		132	33203.7		33.50	431.84	26, 0*
106	30047.3		29.38	734.89		133	33318.2		30.30	824.67	
107	30073.7	30092.2	31.36	661.26	0,16 ?	134	33470.4		26.78	512.11	
108	30104.5		30.68	687.38		135	33610.6		30.63	733.09	
109	30398.3		31.38	507.86	23, 0* ?	136	33697.8		30.41	535.97	
110	30532.0		30.47	468.83		137	33709.4		27.75	564.35	
111	30580.9	30705.4	31.82	998.07	1,15 ?	138	33931.6		29.62	618.68	
112	30640.7		29.78	367.66		139	34104.7		35.41	394.39	27, 0*
113	30682.2		28.06	662.16		140	34139.7	34162.2	30.81	959.49	0,18 ?
114	30980.7	31324.5	31.56	946.35	2,14 ?	141	34203.5		28.33	791.70	
115	31108.3		26.17	473.33		142	34474.1		29.79	405.12	
116	31313.8		31.22	681.42		143	34669.9		30.27	557.33	
117	31368.5		31.33	591.09	24, 0* ?	144	34676.5		29.75	834.31	
118	31427.6		30.09	544.04		145	34738.3		30.87	817.54	
119	31614.4		30.81	539.23		146	34836.1		29.68	500.15	
120	31706.8		26.77	651.43		147	35010.8		36.39	346.82	28, 0*
121	31871.7		27.69	740.79		148	35100.8		32.48	859.62	
122	32124.4	32140.5	31.47	982.69	0,17 ?						

TABLE II. Converged quantum mechanical eigenvalues for non-rotating $(C_{2v})H_3^+$ on the MBB potential energy surface. All notation as in Table I. The zero point energy is 3050.07 cm^{-1}.

N	E_Q	E_{SC}	B_j	B_l	(ν_1,ν_2)	N	E_Q	E_{SC}	B_j	B_l	(ν_1,ν_2)
1	0.0		42.08	44.80	0,0	17	12282.6		26.56	352.94	0,6
2	2525.3		39.70	48.76	0,1	18	12469.6		37.88	40.85	4,0
3	3260.1		41.04	43.59	1,0	19	12681.4		33.49	71.62	2,3 ?
4	4877.1		37.16	55.02	0,2	20	13437.1		28.13	202.98	1,5 ?
5	5638.5		38.91	47.51	1,1 ?	21	13505.2		35.28	54.92	3,2 ?
6	6424.1		39.99	42.51	2,0	22	13771.1		26.57	600.16	0,7
7	7044.1		34.49	65.75	0,3	23	14369.0		35.97	52.60	4,1 ?
8	7863.2		36.59	53.89	1,2 ?	24	14442.2		30.60	136.55	2,4 ?
9	8650.9		38.07	46.62	2,1 ?	25	14923.7		26.40	370.92	1,6
10	9009.6		31.66	88.22	0,4	26	15313.1		32.86	93.10	
11	9493.7		38.94	41.57	3,0	27	15350.8		36.75	41.55	5,0
12	9921.9		33.97	66.10	1,3 ?	28	15379.6	15386.9	27.66	774.31	0,8
13	10734.9		34.26	75.81		29	16009.4		28.40	281.26	
14	10755.9		30.44	134.41	0,5 ?	30	16163.2		34.02	70.59	4,2 ?
15	11563.1		37.18	46.29	3,1 ?	31	16393.5		26.20	545.52	1,7 ?
16	11787.7		31.01	100.17	1,4 ?	32	16946.0		30.26	208.71	

TABLE II (*continued*).

N	E_Q	E_{SC}	B_j	B_l	(ν_1,ν_2)	N	E_Q	E_{SC}	B_j	B_l	(ν_1,ν_2)
33	17079.9		34.65	67.65	5,1?	65	23563.1		30.98	188.44	
				or	11,0*?	66	23867.6		29.03	686.83	
34	17134.4	17140.7	28.41	858.63	0,9	67	23916.6		30.76	435.62	
35	17509.1		26.97	379.15	2,6 ?	68	23977.8		27.09	487.24	
36	17822.5		31.66	141.47		69	24309.9		30.56	133.21	17,0* ?
37	17951.5	18075.6	27.37	721.49	1,8	70	24509.7	24946.2	28.16	701.77	3,9 ?
38	18126.3		35.68	41.71	6,0	71	24672.8		29.89	409.40	
39	18476.1		29.10	340.87		72	24835.0	24850.9	27.97	977.75	0,13
40	18710.3		32.50	119.76		73	24918.0		27.93	410.65	
41	18964.2		27.21	626.90		74	25227.8		32.19	193.26	
42	19006.7	18998.1	27.50	769.66	0,10 ?	75	25318.5	25440.6	28.55	937.61	1,12 ?
43	19346.8		29.92	285.88		76	25392.5		25.71	500.19	
44	19642.9		32.00	300.24		77	25560.6		29.89	392.49	
45	19666.1	19742.6	29.88	601.15	1,9 ?	78	25742.1	26044.0	28.81	889.18	2,11
46	20007.6		28.55	389.59		79	25848.8		29.41	350.93	
47	20239.3		29.85	211.60		80	26154.5		32.41	214.78	
48	20475.1	20764.3	26.95	640.38	2,8 ?	81	26214.3		29.76	614.36	
49	20744.7		33.69	99.64		82	26263.9		28.31	542.00	
50	20878.1		30.24	333.17		83	26543.5		27.98	231.93	
51	20912.2	20922.9	28.65	958.87	0,11	84	26790.8	26808.3	27.39	954.51	0,14 ?
52	21158.9		31.33	169.58		85	26828.2		29.08	590.65	
53	21464.1	21572.3	28.32	754.98	1,10 ?	86	26853.2		28.84	473.82	20,0* ?
54	21531.5		28.56	563.57		87	27113.2		27.93	451.72	
55	21657.3		30.22	341.61		88	27296.0	27411.2	28.37	965.58	1,13 ?
56	22055.2		31.80	157.93	15,0* ?	89	27334.5		31.32	200.07	
57	22121.8	22344.4	28.57	716.00	2,9 ?	90	27637.0		28.69	796.42	
58	22385.8		30.08	390.45		91	27686.9		28.95	524.36	
59	22613.0		28.17	315.82		92	27807.2		28.21	502.11	
60	22867.8	22882.7	28.40	974.66	0,12	93	27892.5		28.53	472.73	21,0*
61	22949.0		27.42	514.00		94	28029.6	28604.6	28.35	827.40	3,11 ?
62	23071.5		30.80	264.31	16,0* ?	95	28251.7		32.52	135.29	
63	23286.3		30.41	296.21		96	28478.0	29295.0	28.37	692.57	4,10 ?
64	23378.0	23483.4	28.80	936.72	1,11	97	28533.4		28.76	396.94	

TABLE III. Rotational (j) dependence of quantum energies of horseshoe states on the DIM surface. Panel a is for horseshoe fundamentals ($\nu_1 = 0$), panel b is for the first excited ($\nu_1 = 1$) state. Missing entries imply that these states could not be assigned. All energies are in cm^{-1} relative to the ground state at the given j. The ground state energies for $j = 5,10,20$ are 1128.65, 3899.00, and 12 317.27 cm^{-1} relative to the ground state at $j = 0$.

$j=$	5		10		20	
ν_2	E	B_j	E	N_j	E	B_j
(a): $\nu_1 = 0$						
1	3 362.5	36.06	3 307.7	31.99	2 826.4	19.29
2	5 412.0	34.38	5 218.9	30.20	3 101.0	21.78
3	6 634.0	35.36	6 520.3	31.22	4 479.7	19.95
4	8 537.1	33.55	8 260.9	28.76	5 648.6	18.48
5	9 808.8	34.55	9 616.4	29.79	7 338.4	18.92
6	11 536.4	32.26	11 083.6	25.66	9 016.7	20.06
7	12 469.4	26.94	11 776.0	25.05	10 617.3	18.83
8	14 355.6	29.69	13 727.1	24.75	12 352.6	19.11
9	15 911.6	30.54	15 435.5	26.38	14 352.6	18.74

TABLE III (*continued*).

$j=$	5		10		20	
ν_2	E	B_j	E	N_j	E	B_j
10	17 758.5	28.44	17 124.2	25.35	16 168.1	18.20
11	19 648.9	27.13	19 366.4	24.78	18 253.9	19.68
12	21 692.5	27.11	21 241.6	25.71		
13	23 754.1	28.78			22 005.9	14.94
14	25 955.7	28.01	25 432.5	25.22	23 980.8	18.51
15	27 863.4	25.98	27 360.3	24.91	26 084.6	19.93
16	30 183.0	29.47	29 412.5	23.93		
(b): $\nu_1 = 1$						
1	6 133.7	31.22	5 690.4	27.15	5 325.0	19.34
2	7 865.2	28.98	7 260.4	25.55	6 106.4	20.95
3	9 430.7	27.48				
4						
5			11 605.6	25.83	10 098.0	17.90
6	14 011.7	27.42			11 808.1	19.08
7			14 672.1	24.91	13 138.9	18.64
8			16 303.0	24.70	14 950.1	18.92
9	18 648.5	29.76	18 089.0	25.61	16 776.6	18.65
10	20 415.9	27.66	19 991.9	24.52	19 070.3	18.21
11	22 306.0	28.33	21 865.7	24.10	20 758.7	19.41
12	24 368.7	29.32			22 765.4	17.55
13	26 343.0	28.74	26 196.9	23.88	24 841.7	19.73
14	28 411.6	24.74	28 078.5	23.95		
15			30 339.1	26.28		

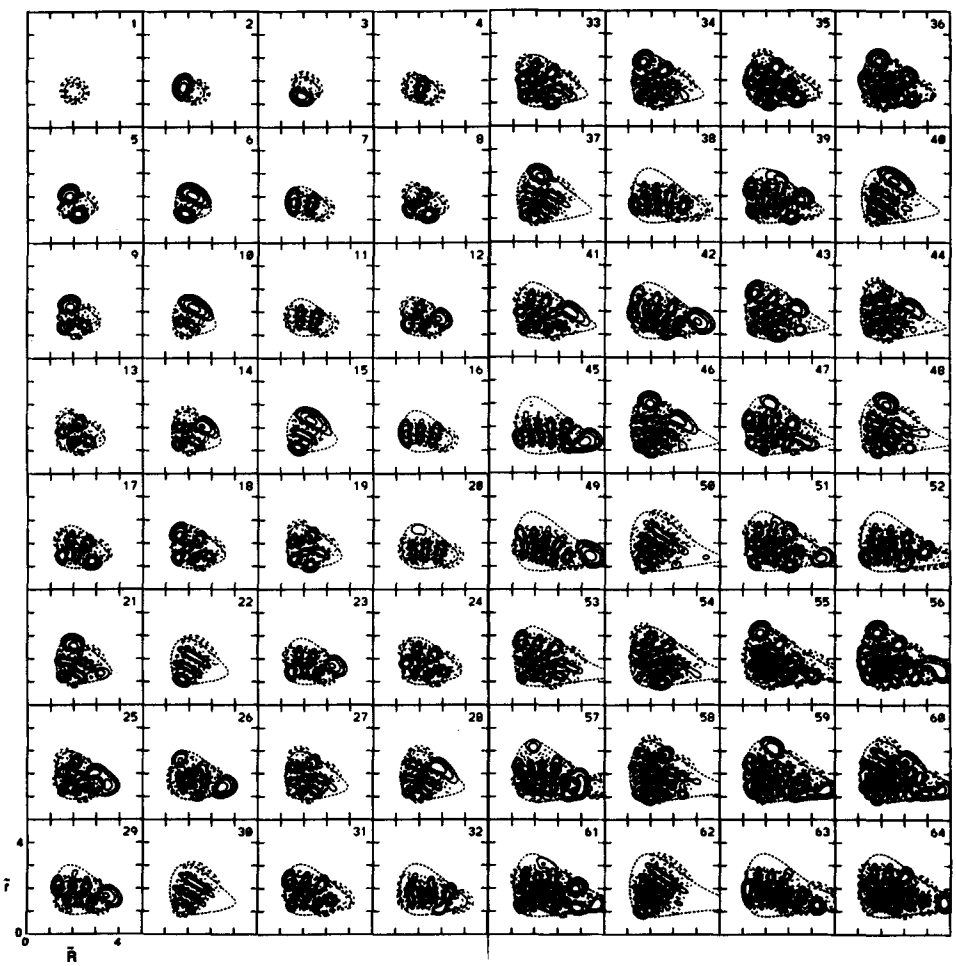

FIG. 2. Bound states of orbiting (C_{2v}) H_3^+ at $l = 20$, on the DIM potential energy surface. Notation is as in Fig. 1.

TABLE IV. Converged eigenvalues for orbiting ($l = 20$) (C_{2v}) H_3^+ on the DIM potential energy surface. All energies are in cm^{-1} relative to the ground state at $l = 20$, whose energy is 13 397.91 cm^{-1} relative to the ground state at $l = j = 0$. Other notation as in Table I.

N	E_Q	B_j	B_ℓ	(ν_1,ν_2)	N	E_Q	B_j	B_ℓ	(ν_1,ν_2)
1	0.0	43.35	26.15	0, 0	33	18669.1	39.45	25.50	3, 4 ?
2	2636.0	43.16	25.82	0, 1	34	19026.8	38.24	26.51	4, 3 ?
3	3193.2	42.32	26.00	1, 0	35	19333.3	40.77	23.01	
4	5192.7	43.09	25.30	0, 2	36	19392.8	39.55	23.81	
5	5753.2	42.02	25.94	1, 1 ?	37	19799.4	37.16	24.73	6, 1 ?
6	6283.5	41.34	25.75	2, 0	38	20015.0	44.51	18.72	0, 9
7	7658.0	43.12	24.59	0, 3	39	20263.1	41.10	22.23	2, 6 ?
8	8255.7	41.86	25.67	1, 2 ?	40	20341.8	36.97	23.53	7, 0
9	8758.3	40.95	25.93	2, 1 ?	41	20869.7	39.85	24.18	3, 5 ?
10	9276.4	40.40	25.41	3, 0	42	21161.9	43.33	20.06	
11	10020.4	43.24	23.72	0, 4	43	21319.2	38.53	25.79	
12	10686.4	41.83	25.12	1, 3 ?	44	21581.5	37.19	26.50	
13	11196.7	40.68	25.96	2, 2 ?	45	21671.6	44.70	17.51	0,10
14	11659.3	39.94	25.78	3, 1 ?	46	21903.1	36.71	25.42	6, 2 ?
15	12175.7	39.50	25.01	4, 0	47	22223.5	40.96	21.59	2, 7 ?
16	12271.4	43.42	22.74	0, 5	48	22346.6	36.60	24.02	7, 1 ?
17	13026.8	41.92	24.30	1, 4 ?	49	22716.8	45.44	17.48	0,11
18	13587.9	40.58	25.65	2, 3 ?	50	22881.5	36.10	23.05	8, 0
19	14022.9	39.57	26.11	3, 2 ?	51	22990.5	40.48	22.15	3, 6 ?
20	14402.6	43.54	21.80	0, 6	52	23274.8	43.65	17.79	1, 9 ?
21	14465.1	39.11	25.38	4, 1 ?	53	23523.7	38.53	24.82	4, 5 ?
22	14984.7	38.58	24.57	5, 0	54	23818.2	37.12	26.96	9, 0 ?
23	15260.6	42.09	23.31	1, 5 ?	55	23986.8	40.31	22.31	
24	15905.8	40.68	24.88	2, 4 ?	56	24061.1	39.75	22.51	
25	16358.0	40.08	25.37	3, 3 ?	57	24173.4	44.30	17.99	0,12 ?
26	16423.7	43.25	21.35	0, 7 ?	58	24364.9	35.90	24.85	7, 2 ?
27	16744.7	38.53	26.04	4, 2 ?	59	24766.3	40.12	20.66	
28	17173.8	38.09	25.13	5, 1 ?	60	24798.7	38.39	21.42	
29	17376.3	42.31	22.22	1, 6 ?	61	25034.0	40.44	20.69	
30	17705.3	37.69	24.09	6, 0	62	25346.4	35.04	22.58	9, 0
31	18111.2	41.26	23.44	2, 5 ?	63	25474.1	44.93	17.71	0,13 ?
32	18309.5	43.93	19.82	0, 8	64	25602.4	40.61	21.67	

difference between the semiclassical prediction and the exact quantal result. Here one notes that for all states assigned as $(0,\nu_2)$ there is a negligible deviation. However, the deviation does increase with the ν_1 quantum number. This is clearly a reflection of the breakdown of the harmonic approximation which is based on the harmonic stability frequency. A more accurate estimate of the excited ν_1 states could be obtained using the adiabatic method proposed in Ref. 19. However this is beyond the scope of the present analysis.

For the restricted C_{2v} problem, the horseshoe orbit exists and is stable for almost all energies above the collinear threshold. This is not the case for the inverted hyperspherical mode. In Fig. 4 we show orbits which are relevant for the quantum localization shown in Fig. 1. Again there is agreement between the quantum localization and the classical orbits, however it is evidently not as good as for the horseshoe mode. Furthermore, we do not find a classical counterpart for every quantum localization. In fact, it is somewhat misleading to put all of the inverted hyperspherical states into one group. At low energies, the relevant orbit stays within the half plane and does not cross the $R = 0$ axis. The frequency of this orbit is very different from its more complicated extension at high energies, close to dissociation. Moreover this family changes stability a number of times. The gap

TABLE V. Properties of periodic orbits. Energies, frequencies, and rotational constants are in cm^{-1}. Energies are relative to the bottom of the well. Actions are in units of $2\pi\cdot\hbar$. Numbers in parentheses are for the MBB surface, all other entires are for the DIM surface. Note that for the DIM surface, the collinear threshold (below which horsehoe orbits do not exist) is at 12 347.3 cm^{-1} and the dissociation energy into $H^+ + H_2$ is 39 713.1 cm^{-1}. The collinear threshold on the MBB surface is 14 275.5 cm^{-1}. This surface is not accurate for energies above ~30 000 cm^{-1}.

Property	E	$j=0$		$j=2$	$j=5$	$j=8$	$j=10$
Action	18 000	(18.51)	20.05	20.18	20.83	21.95	22.91
	20 000	(20.70)	22.14	22.27	22.90	23.97	24.87
	25 000	(25.85)	27.08	27.21	27.81	28.82	29.64
	30 000	(30.97)	31.88	32.00	32.60	33.57	34.35
	35 000		36.75	36.87	37.47	38.42	39.18
	40 000		41.81	41.94	42.54	43.48	44.22
Frequency	18 000	(888.10)	930.96	929.27	920.05	901.10	881.47
	20 000	(940.21)	977.02	975.85	969.34	955.84	942.11
	25 000	(983.66)	1036.04	1035.62	1033.06	1026.94	1020.17
	30 000	(964.51)	1040.16	1040.58	1040.18	1038.84	1036.00
	35 000		1010.60	1010.90	1012.66	1012.86	1012.54
	40 000		963.57	963.93	965.44	967.08	967.71
Rotational constant B_j	18 000	(28.18)	30.49	30.28	29.26	27.63	26.34
	20 000	(28.63)	31.25	31.04	30.00	28.35	27.07
	25 000	(28.26)	32.18	31.95	30.83	29.11	27.79
	30 000	(26.95)	32.15	31.85	30.70	28.87	27.55
	35 000		31.50	31.23	29.87	28.06	26.70
	40 000		30.47	30.18	28.82	26.88	25.50
Absolute stability frequency	18 000	(2638.8)	2819.0	2820.7	2824.3	...	...
	20 000	(2583.8)	2783.4	2783.6	2785.0	...	...
	25 000	(2558.3)	2709.7	2704.4	2709.3	...	...
	30 000	(2561.1)	2684.7	2726.3	2735.2	2707.4	...
	35 000		2666.8	2689.2	2689.1	2684.6	...
	40 000		2628.9	2638.2	2636.9	2635.2	2634.8

in assigned hyperspherical quantum states, on the DIM surface between the (11,0) and (19,0) states is a reflection of this instability. The hyperspherical orbit is not stable when perturbed in the full 3D space and so probably not as significant as the horseshoe mode, and so does not warrant a very detailed study.

Finally, we have also studied the periodic orbits for the $l=20$ case. Here we find that the symmetric stretch and bend (horseshoe) periodic orbits are stable (within the restricted C_{2v} subspace) at almost all energies below the dissociation threshold in agreement with the regularity found in the quantum states. We have also studied the full 3D proper-

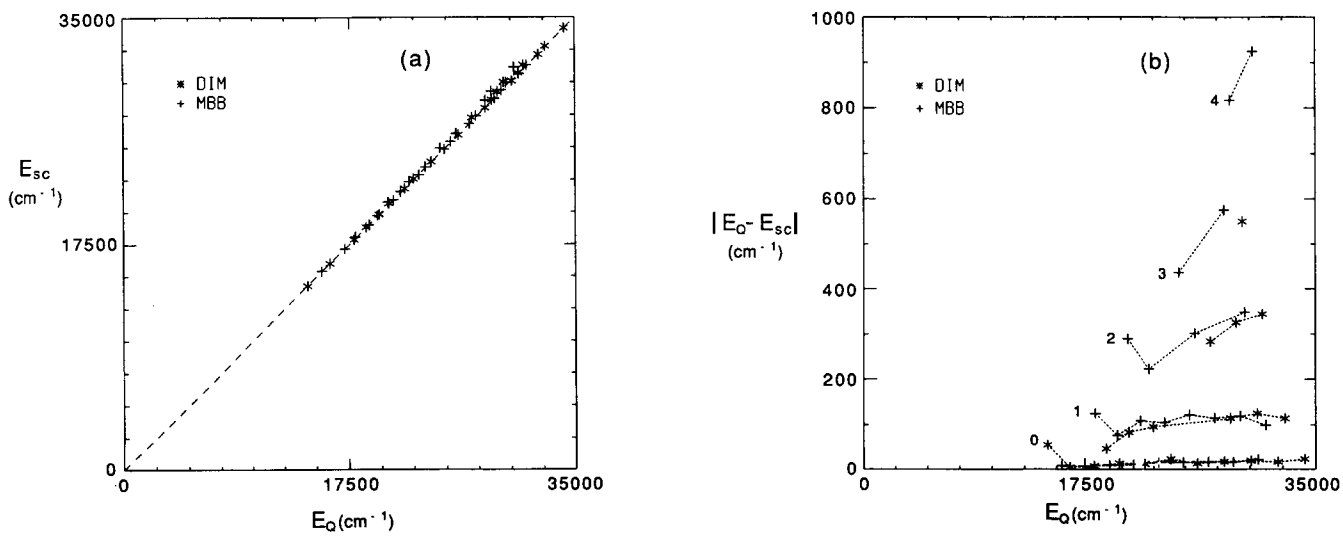

FIG. 3. Accuracy of semiclassical quantization of horseshoe orbits. In panel a we plot the predicted semiclassical energy against the exact quantal energy for all horseshoe states appearing in Tables I and II. The dashed line (unit slope) represents exact agreement. A more detailed view is presented in panel b where the energy difference is plotted for different excitations ($\nu_1 = 0$–4) perpendicular to the orbit. Results are shown for both surfaces and based on Tables I and II.

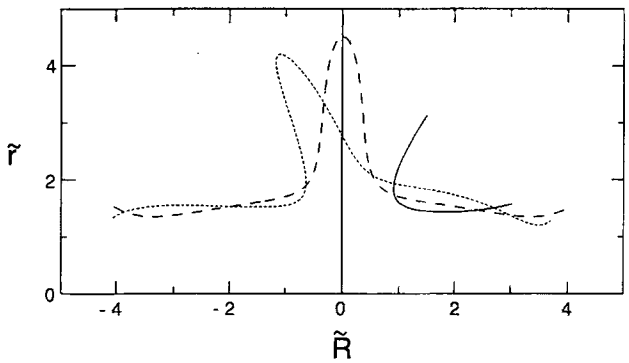

FIG. 4. Inverted hyperspherical orbits. Three stable orbits in the C_{2v} ($j = l = 0$) subspace are plotted. The solid line is (relative to the bottom of the well) at $E = 18\,663\ \mathrm{cm}^{-1}$, the dotted line at $E = 31\,676\ \mathrm{cm}^{-1}$ and the dashed line at $E = 31\,683\ \mathrm{cm}^{-1}$. All orbits are on the DIM surface. Note the similarity to the states numbered 36 and 109.

ties of the symmetric and horseshoe periodic orbits for $l = 20$. As in previous work based on an adiabatic switching method,[9] we find that all these orbits are unstable for energies at least greater than 0.5 eV below the $H_2 + H^+$ dissociation threshold. To gain further insight into this instability we studied the properties of these orbits in 3D with, and without Coriolis coupling. When the Coriolis coupling terms are left out of the Hamiltonian (as done for example in Ref. 20) the $l = 20$ orbits are stable. We thus conclude that Coriolis coupling is the source of instability for these orbiting states. This is not too surprising, at $l = 20$, the orbiting frequency is of the same order of magnitude as the vibrational frequencies.

IV. DISCUSSION

The most striking feature of the present study is that the horseshoe mode has a profound effect on the quantum mechanical spectrum of reduced dimensionality H_3^+. In agreement with expectations based on classical stability analysis, we find a localization of quantum states around the horseshoe periodic orbit, moreover, a simple semiclassical quantization of the horseshoe orbit gives excellent predictions for the exact quantum states. This localization exists even though classical motion at high energies close to dissociation is predominantly chaotic and the stable phase space surrounding the horseshoe orbits is small.

The robustness of this mode suggests that it is not unique to H_3^+. Elsewhere[21] we will provide details on a study of isotopes of H_3^+ where we also find that the horseshoe mode is stable. It should be of interest to study other triatomic molecules whose equilibrium configuration has a C_{2v} symmetry and the collinear configuration is a saddle point on the potential energy surface.

Our study of the C_{2v} configuration was motivated by the suggestion that the horseshoe mode underlies the coarse grained spectrum measured in the photodissociation experiments of Carrington and Kennedy. The prominence of the horseshoe mode implies that at least the coarse grained absorption spectrum for the restricted C_{2v} geometry should have prominent peaks that correspond to the frequency of the horseshoe mode. This would then be in agreement with the Feshbach analysis of Taylor and co-workers,[10] who suggested that weakly stable periodic orbits provide a ladder of states which strongly enhance the absorption. A detailed study of the quantum and classical, C_{2v} restricted, absorption spectrum, at energies close to dissociation will be presented elsewhere.[21]

Although the restricted study does provide insight into the dynamics of floppy molecules, it is not sufficient. Based on the C_{2v} study one might have concluded that orbiting states are extremely important for understanding the full 3D spectrum since they seem to be very regular. It is only through the full 3D classical mechanical study of stability of the orbits that we can negate this observation. We stress that in 3D only the horseshoe orbits are stable. Thus a restricted study can suggest possible localizations, but only a full 3D computation can verify which motion really is important and which is not.

Finally we note, that quantum mechanics are much more illuminating than classical mechanics! It is only as a result of the quantal study that we came across the inverted hyperspherical mode for this system. The quantum wave functions immediately provide a global picture, which classical mechanically is obtained through a very tedious search for periodic orbits. On the other hand, a full 3D quantum study at high J values is still impossible. We expect that a combination of classical and quantum mechanical studies as presented in this paper will be very useful for understanding the dynamics of other small molecules at high energy.

ACKNOWLEDGMENTS

This work has been supported by a grant of the U. S.–Israel Binational Science Foundation. Calculations were performed on the Convex C-220 computer of the Weizmann Institute Computer Center.

[1] J. K. G. Watson, S. C. Foster, A. R. W. McKellar, P. Bernath, T. Amano, F. S. Pan, M. W. Crofton, R. S. Altman, and T. Oka, Can. J. Phys. **62**, 1875 (1984), and references therein; L. W. Xu, M. Bawendi, B. D. Rehfuss, C. Gabrys, and T. Oka, 44th Symposium on Molecular Spectroscopy, Columbus, Ohio, Paper RA3 (1989).
[2] G. D. Carney and R. N. Porter, J. Chem, Phys. **65**, 3547 (1976).
[3] W. Meyer, P. Botschwina, and P. G. Burton, J. Chem. Phys. **84**, 891 (1986).
[4] S. Miller and J. Tennyson, J. Mol. Spectrosc. **126**, 183 (1987), **128**, 530 (1988), **136**, 223 (1989).
[5] R. M. Whitnell and J. C. Light, J. Chem. Phys. **90**, 1774 (1989).
[6] A. Carrington and R. M. Kennedy, J. Chem. Phys. **81**, 91 (1984).
[7] R. Pfeiffer and M. S. Child, Mol. Phys. **60**, 1367 (1987).
[8] M. Berblinger, E. Pollak, and Ch. Schlier, J. Chem. Phys. **88**, 5643 (1988).
[9] J. M. Gomez Llorente and E. Pollak, J. Chem. Phys. **89**, 1195 (1988), **90**, 5406 (1989).
[10] H. S. Taylor, J. Zakrzewski, and S. Saini, Chem. Phys. Lett. **145**, 555 (1988); J. M. Gomez Llorente, J. Zakrzewski, H. S. Taylor, and K. C. Kulander, J. Chem. Phys. **90**, 1505 (1989).
[11] R. H. Bisseling, R. Kosloff, J. Manz, F. Mrugala, J. Römelt, and G. Weichselbaumer, J. Chem. Phys. **86**, 2626 (1987).
[12] K. Stefanski and E. Pollak, Chem. Phys. **134**, 37 (1989).
[13] K. Stefanski and E. Pollak, J. Chem. Phys. **87**, 1079 (1987).
[14] J. Tennyson and B. T. Sutcliffe, J. Chem. Phys. **77**, 4061 (1982).

[15] J. Tennyson and B. T. Sutcliffe, J. Mol. Spectrosc. **101**, 71 (1983).
[16] R. K. Preston and J. C. Tully, J. Chem. Phys. **54**, 4297 (1971).
[17] E. Pollak in *Theory of Chemical Reaction Dynamics*, edited by M. Baer (CRC, Boca Raton, FL, 1985), Vol. 3, p. 123.
[18] M. Hénon, Physica D **5**, 412 (1982).
[19] B. Eckhardt, G. Hose, and E. Pollak, Phys. Rev. A **39**, 3776 (1989).
[20] G. Brocks and J. Tennyson, J. Mol. Spectrosc. **99**, 263 (1983).
[21] Work in progress.